Journal of Power Sources 195 (2010) 5176–5184

Contents lists available at ScienceDirect

Journal of Power Sources

journal homepage: www.elsevier.com/locate/jpowsour

Evaluation of $Ba_{0.6}Sr_{0.4}Co_{0.9}Nb_{0.1}O_{3-\delta}$ mixed conductor as a cathode for intermediate-temperature oxygen-ionic solid-oxide fuel cells

Cheng Huang, Dengjie Chen, Ye Lin, Ran Ran, Zongping Shao*

State Key Laboratory of Materials-Oriented Chemical Engineering, College of Chemistry & Chemical Engineering, Nanjing University of Technology, No. 5 Xin Mofan Road, Nanjing 21009, PR China

ARTICLE INFO

Article history:
Received 21 January 2010
Received in revised form 25 February 2010
Accepted 25 February 2010
Available online 3 March 2010

Keywords:
Perovskite
Cathode
Solid-oxide fuel cells
Mixed conductors

ABSTRACT

A perovskite-type $Ba_{0.6}Sr_{0.4}Co_{0.9}Nb_{0.1}O_{3-\delta}$ (BSCN) oxide is investigated as the cathode material of oxygen-ionic solid-oxide fuel cells (SOFCs) with $Sm_{0.2}Ce_{0.8}O_{3-\delta}$ (SDC) electrolyte. Powder X-ray diffraction and SEM characterization demonstrate that solid phase reactions between BSCN and SDC are negligible at temperatures up to 1100 °C. The results of thermal-expansion and electrical conductivity measurements indicate the introduction of Ba^{2+} into the A-site of $SrCo_{0.9}N_{0.1}O_{3-\delta}$ (SCN) led to a decrease in the thermal-expansion coefficient (TEC) and electrical conductivity of the compound. A TEC of $14.4 \times 10^{-6}\,K^{-1}$ is observed for BSCN within a temperature range of 200–500 °C. The chemical diffusion coefficient (D_{chem}) and surface exchange constant (k_{ex}) of BSCN and SCN are obtained using an electrical conductivity relaxation technique and BSCN prove to have higher D_{chem} and k_{ex} than SCN. An area-specific resistance of $0.1\,\Omega\,cm^{-2}$ is achieved for BSCN cathodes at 600 °C based on symmetric cells test. Peak power density of ~1150 mW cm^{-2} is reached for a thin-film electrolyte cell with BSCN cathode at 600 °C, which is higher than a similar cell with SCN cathode (~1008 mW cm^{-2}). BSCN is a promising cathode material for oxygen-ionic IT-SOFCs.

1. Introduction

Ceramic oxides with mixed oxygen-ionic and electronic conductivity are a type of functional material that can conduct oxide ions and electrons simultaneously at elevated temperatures. These materials have potential applications such as dense ceramic membranes for oxygen separation from air or as membrane reactors for coupling the oxidation of light hydrocarbons to value-added products [1–4]. Many mixed conducting composite oxides have been developed for ceramic oxygen separation membranes with high oxygen permeability at elevated temperatures [5–10]. However, during the past decade, mixed conducting oxides have also received considerable attention as cathode materials of solid-oxide fuel cells (SOFCs) [11–16]. In SOFCs, with electrodes composed of pure electronic conductors such as $La_{0.8}Sr_{0.2}MnO_3$ (LSM), oxygen reduction is limited to the electrode–electrolyte–air triple phase boundary (TPB) region. However, the active site is effectively extended to the entire exposed cathode surface if a mixed conductor is used as the cathode material. Consequently, the electrode activity for oxygen reduction may be improved over the LSM electrode, especially at reduced temperatures.

Over the past several years, we have demonstrated that mixed conductors that show high oxygen permeability at elevated temperatures perform well as cathodes of SOFCs at intermediate temperatures [17–21]. For example, $Ba_{0.5}Sr_{0.5}Co_{0.8}Fe_{0.2}O_{3-\delta}$ (BSCF) composite oxide was initially developed as a material for high-temperature oxygen separation membranes [17]. However, BSCF was later demonstrated to be a highly promising cathode material for intermediate-temperature solid-oxide fuel cells (IT-SOFCs), with high activity for oxygen reduction at temperatures of 500–600 °C [18]. Fig. 1 shows schematically the reduction of oxygen over a mixed conducting electrode and oxygen permeation through a dense mixed conducting ceramic membrane. Both processes involve the surface exchange and bulk diffusion of oxygen. However, for oxygen separation applications, the ceramic membranes are typically dense membranes with a thickness at the millimeter level. The mixed conductors are prepared as a porous structure with an effective thickness of only about 20 μm when used as cathodes of SOFCs for oxygen reduction. This implies the importance of surface exchange and bulk diffusion in mixed conductors, which may play a different role in ceramic oxygen separation membranes and in cathodes of IT-SOFCs. Knowledge about the bulk diffusion and surface exchange properties of mixed conductors would be useful for practical applications. To perform well as a cathode, in addition to a high electrochemical activity for the reduction of oxygen, the material should have a comparable thermal-expansion coefficient (TEC) to the electrolyte, high resistance to reacting with the

* Corresponding author. Tel.: +86 25 83172256; fax: +86 25 83172256.
E-mail address: shaozp@njut.edu.cn (Z. Shao).

0378-7753/$ – see front matter © 2010 Elsevier B.V. All rights reserved.
doi:10.1016/j.jpowsour.2010.02.080

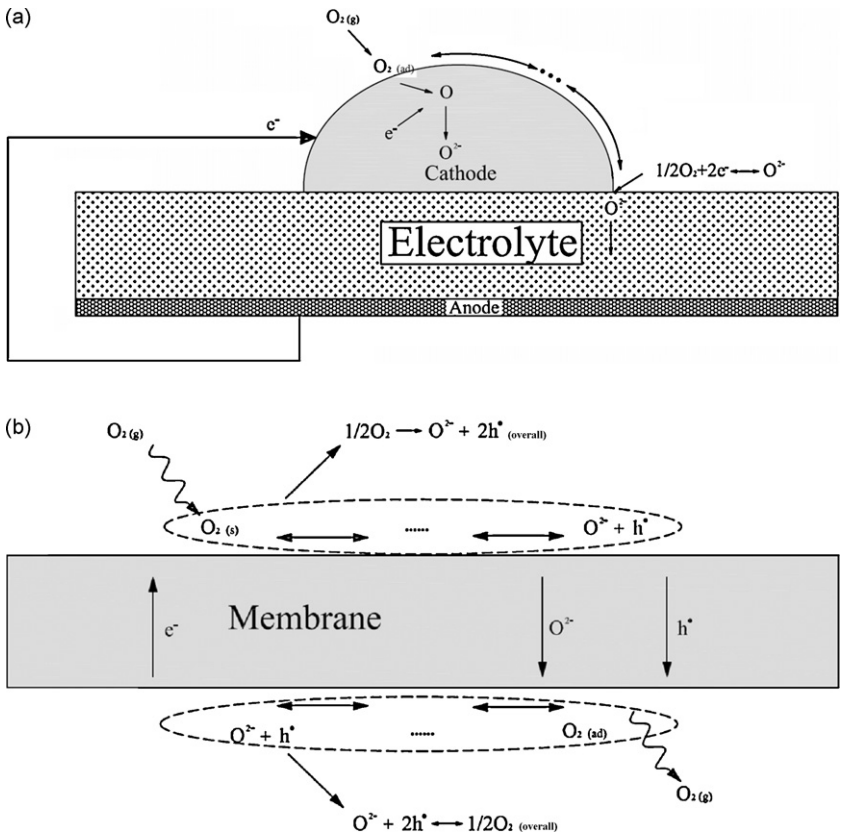

Fig. 1. Schematic of oxygen reduction over a mixed conducting cathode (a), and oxygen permeation through a dense mixed conducting ceramic membrane (b).

electrolyte and good electronic conductivity for efficient current collection.

Recently, strontium niobium cobaltite composite oxides have received much attention as materials in oxygen separation membranes. In particular, $SrCo_{0.9}Nb_{0.1}O_{3-\delta}$ (SCN) was found to possess high chemical stability and oxygen permeability at elevated temperatures [22–24]. Recently, we found that SCN is also a good cathode material for IT-SOFCs. By operating on hydrogen fuel, a peak power density (PPD) of 1008 mW cm^{-2} was achieved for a cell with a thin-film SDC electrolyte (~20 μm), a Ni + SDC anode and a SCN cathode at 600 °C [25]. Very recently, we demonstrated that the oxygen permeability of the membrane was further improved through partial substitution of Sr^{2+} in SCN by Ba^{2+} to yield $Ba_{0.6}Sr_{0.4}Co_{0.9}Nb_{0.1}O_{3-\delta}$ (BSCN), a novel perovskite-type oxide [26].

In this study, the potential application of BSCN as a cathode material in IT-SOFCs with a doped ceria electrolyte was systematically investigated. The chemical diffusion coefficient and surface exchange constant of BSCN and SCN were studied, as well as the reactivity with the SDC electrolyte at high temperatures, the TEC, the conductivity under various atmospheres and the performance of the electrode. The results indicate that BSCN is a highly promising cathode material for IT-SOFCs with SDC electrolyte.

2. Experimental

2.1. Powder synthesis

SDC oxide powder was synthesized by a combined EDTA-citrate complexing sol–gel process. Metal nitrates of $Sm(NO_3)_3{\cdot}6H_2O$ and $Ce(NO_3)_2{\cdot}6H_2O$ were prepared from a mixed solution of Sm^{2+} and Ce^{4+} with a molar ratio of 1:4. EDTA and citric acid were added to the solution to serve as complexing agents with a molar ratio of total metal ions to EDTA to citric acid set at 1:1:2. The pH of the solution was adjusted to 6 with NH_4OH and the water was evaporated slowly from the solution by heating at 90 °C until a transparent gel was obtained, which was pre-fired at 250 °C and further calcined at 800 °C in air for 5 h to yield the final products with the desired lattice structure.

BSCN and SCN composite oxides were synthesized by a mechano-chemical activation-enhanced solid phase reaction with $BaCO_3$, $SrCO_3$, Nb_2O_5 and Co_2O_3 as raw materials and cation sources. The chemicals were weighed and mixed thoroughly using a high-energy ball miller (Fritsch, Pulverisette 6) at a rotational speed of 400 rpm for 3 h in liquid acetone. The slurry was dried in an electrical oven to obtain a solid precursor, which was calcined in air in a two-step procedure, first at 950 °C for 10 h and then at 1100 °C for 5 h, to yield the final products with the desired lattice structure.

2.2. Symmetric cell and fuel cell fabrication

To prepare the symmetric cells for impedance spectroscopy measurements, the BSCN powder was dispersed in a premixed solution of glycol, ethylene glycol and isopropyl alcohol and a colloidal suspension was formed through the use of a high-energy ball miller at a rotational speed of 400 rpm for 0.5 h. The suspension was then symmetrically painted on both surfaces of dense SDC pellets with a diameter of ~13 mm and a thickness of ~0.8 mm and the whole cells were calcined at 950–1100 °C.

Anode-supported single cells for *I–V* polarization tests were fabricated by dry pressing/sintering of the anode–electrolyte dual-layer cells and spray deposition/firing of the cathode layer. Anode powder, composed of 60 wt.% NiO and 40 wt.% SDC, was pressed into a substrate disk using a stainless steel die under a hydraulic pressure of 120 MPa. Next, SDC powder calcined at 800 °C was distributed over the anode surface homogenously and pressed at

240 MPa to form a green dual-layer cell. The cell was sintered at 1450 °C for 5 h to achieve densification of the electrolyte layer and a firm connection between the anode and the electrolyte layers. The cathode layer was deposited over the electrolyte surface by air-driven spray deposition of a cathode colloidal suspension. Next calcination at 1000 °C for 2 h was conducted to form a well-connected cathode network and good adhesion of the cathode layer to the electrolyte layer. The resulting coin-shaped cathode had an effective geometric surface area of 0.48 cm^2.

2.3. Basic characterization

XRD patterns of the powders were analyzed by a diffractometer (Bruker D8 Advance) equipped with Cu Kα radiation (λ = 1.5418 Å). Diffraction patterns were collected at room temperature by step scanning angles (2θ) between 20 and 80°. The microscopic features of the sintered electrodes were characterized by an Environmental Scanning Electron Microscope (ESEM, QUANTA-2000). Electrical conductivity was measured using a four-probe DC technique under various atmospheres, using Ag paste as a current collector. Prepared powders were ball-milled and subsequently pressed into green bars (8 mm × 2 mm × 5 mm) with a stainless steel die under a hydraulic pressure of 200 MPa. The green bar was densified by sintering at 1120 °C for 5 h. Silver paste was applied to each bar and four wires were attached to the edge of the bar as a current and voltage probe. Measurements were conducted by a Keithley 2420 meter with a temperature interval of 10 °C, from 300 to 900 °C. The TEC of the sintered sample was measured by a dilatometer (Netsch DLL 402C/3/G) from room temperature to 900 °C, with an air-purge flow rate of 50 ml min^{-1} [standard temperature and pressure, STP]. To conduct the oxygen temperature-programmed desorption (O_2-TPD) experiment, 0.15 g of oxide powder was placed inside a U-type quartz reactor with an inner diameter of approximately 3 mm. A K-type thermocouple was placed near the oxide powders for temperature control and monitoring. High purity helium (>99.99%) was introduced to the reactor at a flow rate of 20 ml min^{-1} [STP]. After flushing the system with helium for 30 min at room temperature to eliminate weakly absorbed species on the surface, the reactor was heated to 930 °C at a rate of 10 °C min^{-1}. During the heating process, oxygen was released from the oxide lattice and collected by the helium and sent to the mass spectrometer (Hiden QIC-20) for *in-situ* analysis.

2.4. Electrical conductivity relaxation

The D_{chem} and k_{ex} were obtained by the electrical conductivity relaxation (ECR) method. A bar with dimensions of 8 mm × 2 mm × 5 mm was mechanically polished and ultrasonically cleaned prior to the ECR test. The bar was heated in an electrical furnace at a certain temperature under a controlled atmosphere. After stabilization, a sudden change in the oxygen partial pressure, from 0.05 to 0.21 atm, was achieved by switching to another gas. The time dependence of conductivity was measured using a four-probe DC technique. The change in the oxygen partial pressure was achieved by mixing the proper amount of argon and oxygen with mass flow controllers at a flow rate of 300 ml min^{-1} [STP]. The test was conducted between 600 and 450 °C, at an interval of 50 °C. After each change in temperature, the bar was stabilized for at least 1 h.

2.5. Electrochemical characterization

The electrochemical impedance spectra (EIS) of the cells were characterized by an electrochemical workstation Solatron 1287 potentiostat and a 1260A frequency analyzer in a frequency range from 0.1 to 100 kHz, with single amplitude of 10 mV under open cell voltage (OCV) conditions. The oxygen partial pressure was varied between 0.04 and 1 atm. by mixing O_2 (99.99%) and N_2 (99.999%) with mass flow controllers at a flow rate of 200 ml min^{-1} [STP]. The sample was heated to 650 °C and tested between 650 and 450 °C, at an interval of 50 °C. The impedance data were collected using Z-View 2.9c software and analyzed by a complex nonlinear least-square (CNLS) fitting program via Z-Plot 2.9c software.

2.6. I–V polarization test

An in-house constructed fuel cell test station was applied for electrochemical performance evaluation of the fabricated cells. The cell was sealed onto a quartz reactor with humidified (3% H_2O) hydrogen at a flow rate of 80 ml min^{-1} [STP], while ambient air was applied to the cathode atmosphere. *I–V* polarization curves were collected at an interval of 50 °C over a temperature range of 600–450 °C using a digital source meter (Model 2420, Keithley, USA) based on the four-probe configuration.

3. Results and discussion

3.1. Structural compatibility with SDC electrolyte

To prepare the membrane-electrode assemblies (MEAs), the cathode material was deposited onto an electrolyte surface by various physical or chemical techniques. The cells that contain the cathode layer were further fired at an elevated temperature to allow for the firm adhesion of the cathode layer to the electrolyte surface and a tight connection between the electrode particles to minimize contact resistance. However, an interfacial reaction between the electrolyte and cathode layers may occur during the high-temperature firing process. The interfacial layer may cause a diffusion barrier for oxygen ions or protons and lead to a serious deterioration in the performance of the electrode.

The potential phase reaction between BSCN and SDC was investigated by powder reaction, where equal weights of BSCN and SDC in powder form were mixed thoroughly and calcined in air at various temperatures between 950 and 1100 °C for 5 h. The resultant products were later subjected to XRD characterization. As shown in Fig. 2, all samples calcined at different temperatures yielded diffraction peaks that indicated a physical mixture of a perovskite-type BSCN-related phase and a fluorite-type SDC-related phase. Furthermore, there is no obvious peak shift of the BSCN-related phase and the SDC-related phase when compared to single-phase BSCN and SDC respectively. This implies that the phase reaction between BSCN and SDC is not significant at all firing temperatures.

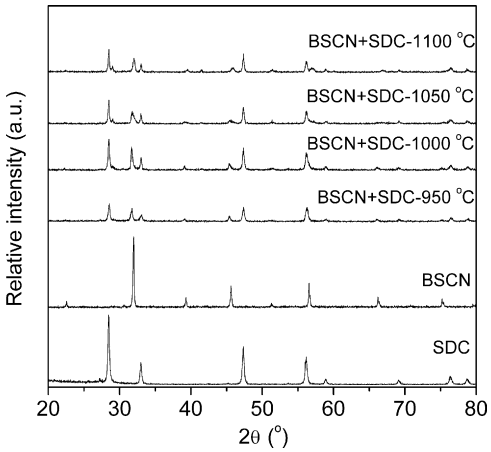

Fig. 2. X-ray diffraction patterns of SDC, BSCN and a BSCN + SDC mixture after calcination at various temperatures in air for 2 h.

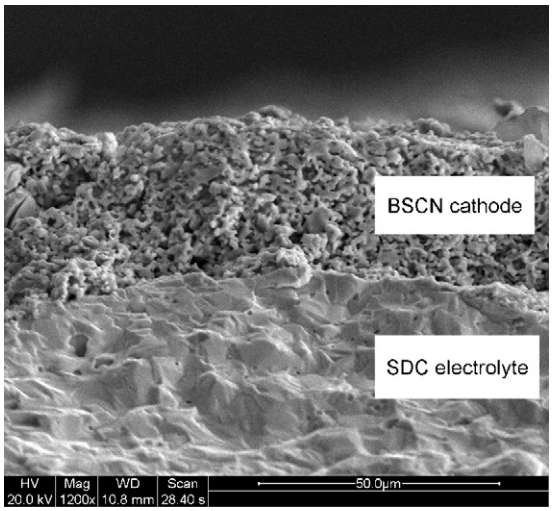

Fig. 3. SEM photo of a BSCN–SDC dual-layer cell from a cross-sectional view after calcination at 1000 °C for 2 h.

As mentioned, the phase reaction between the cathode and the electrolyte may result in the formation of an interfacial layer [27]. To further exploit the potential phase reaction between BSCN and SDC, a porous layer of BSCN was deposited onto the electrolyte surface. The dual-layer cell was then calcined at 1000 °C for 5 h and subjected to SEM for observation. Shown in Fig. 3 are the micrographs of the dual-layer cell from a cross-sectional view. The BSCN layer is attached to the electrolyte surface, suggesting good thermo-mechanical compatibility. There is also no evidence of an obvious interfacial layer between the BSCN cathode and the SDC electrolyte. The results support the absence of a significant phase reaction between BSCN and SDC during the high-temperature fabrication.

3.2. TEC

For practical applications, the cell components should have comparable TEC values. Large differences in TECs may lead a large internal stress induced during the heating and cooling processes, which may negatively affect the cell operational stability. Doped ceria electrolytes typically have a TEC of $11–12 \times 10^{-6}\,K^{-1}$ [28]. Cobalt-based perovskite oxides usually have a high TEC [29–32]. For example, BSCF has a reported TEC of $>21 \times 10^{-6}\,K^{-1}$ between 30 and 1000 °C [31]. Previously, we have demonstrated that the TEC of cobalt-contained perovskite oxides is strongly affected by the dopant and cation stoichiometry [22,33]. Dilatometric measurements up to 900 °C were conducted in air to investigate the thermal-expansion behavior of the BSCN oxide. Fig. 4 shows the corresponding thermal-expansion curve of BSCN and the SCN thermal-expansion curve for comparison. The average TEC values for SCN and BSCN in temperature ranges of 200–500, 200–600, 500–900 and 200–900 °C are presented in Table 1.

For both BSCN and SCN samples, the thermal-expansion curve can be separated into two regions with different slopes, with a transition at 500 °C. For cobalt perovskite oxides such as BSCN, the thermal-expansion could be due to several aspects, including

Table 1
The average TECs of SCN and BSCN at different temperatures.

Δt (°C)	TEC ($\times 10^{-6}\,K^{-1}$) for SCN	TEC ($\times 10^{-6}\,K^{-1}$) for BSCN
200–500	18.4	14.4
200–600	19.0	17.3
500–900	22.1	21.9
200–900	20.3	18.2

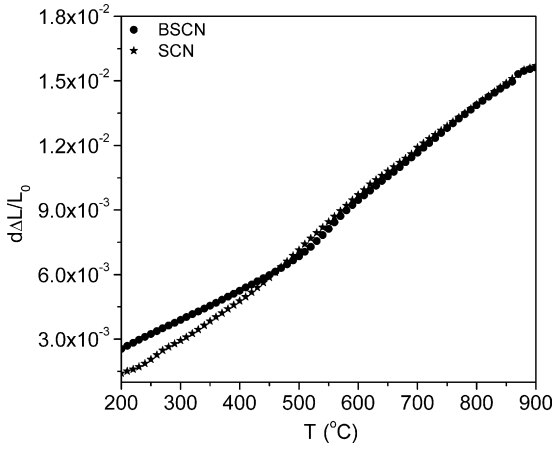

Fig. 4. Thermal-expansion curves of BSCN and SCN collected under an air atmosphere between 200 and 900 °C.

thermal activation of the compositional cations, the electronic spin-state transition associated with the transition from low spin-state ($t_{2g}^6 e_g^0$) to high spin-state ($t_{2g}^4 e_g^2$) Co^{3+} ions and chemical expansion due to the thermal reduction of cobalt ions to a lower valence state. It is well known that cobalt can be thermally reduced to a lower valence state at intermediate temperatures and lead to the simultaneous production of oxygen vacancies and an increase in the ionic size of cobalt. To interpret the transition of thermal-expansion behavior at 500 °C, O_2-TPD analysis of BSCN powder was conducted. As shown in Fig. 5, at 500 °C, a large desorption peak was observed for BSCN, indicating the loss of oxygen in the lattice. The release of oxygen from the oxide was accompanied by the reduction of cobalt to a lower valence state, to maintain electrical charge neutrality. This implies that the change in thermal-expansion behavior at 500 °C was due to the thermal reduction of cobalt in the composite oxide. Within the temperature range of 200–500, 500–900 and 200–900 °C, a calculated TEC of 14.4×10^{-6}, 21.9×10^{-6} and $18.2 \times 10^{-6}\,K^{-1}$ was obtained for BSCN, respectively. As a comparison, the corresponding TEC values were 18.4×10^{-6}, 22.1×10^{-6} and $20.3 \times 10^{-6}\,K^{-1}$ for SCN. The TEC of BSCN was lower than SCN and this is attributed to a smaller loss of oxygen during the heating process, as demonstrated by our previous temperature-programmed oxygen desorption analysis [26]. The thermal-expansion behavior of BSCN and SCN is highly dependent on the investigated temperature range. A sharp increase in TEC was observed at temperatures higher than 500 °C due to an increase in the chemically induced expansion as previously demonstrated.

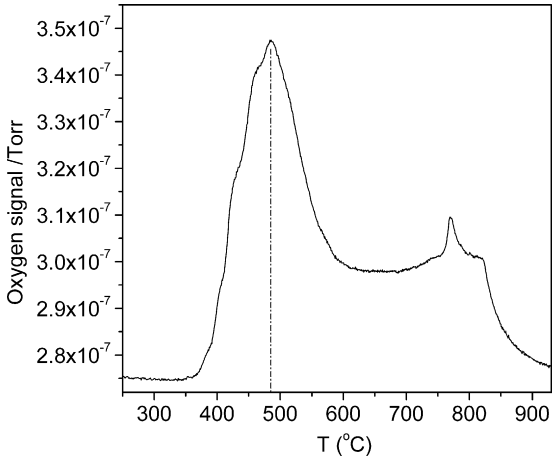

Fig. 5. Typical oxygen temperature-programmed desorption profile of BSCN oxide.

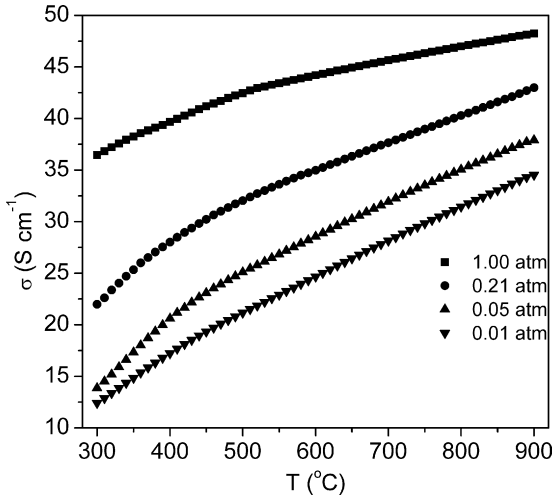

Fig. 6. Electrical conductivity of BSCN under various oxygen partial pressures between 300 and 900 °C.

The small TEC of BSCN between 200 and 500 °C suggests that BSCN is a highly promising cathode for SOFC at operating temperatures less than 500 °C.

3.3. Electrical conductivity

Sufficient electronic conductivity under real operating conditions is of significant importance for the practical application of fuel cell electrodes. Although the fuel cell cathode is typically exposed to an air atmosphere, consumption of oxygen is large at high polarization current densities. Under these conditions, the oxygen potential at the cathode surface could be much lower than the surrounding atmosphere (air). For example, at cathode overpotential of 0.2 V, the apparent oxygen partial pressure over the cathode surface is as low as 5×10^{-6} atm. when the cathode is exposed to an air atmosphere at 600 °C. Because the cathode overpotential increases with an increase in polarization current density, a high electronic conductivity at reduced oxygen concentration is of critical importance to minimize contact resistance.

As shown in Fig. 6, the electrical conductivity of BSCN varies under different oxygen partial pressures and as a function of temperature. Since the electronic conductivity overwhelms the oxygen-ionic conductivity, the reported electrical conductivity reflects the electronic conductivity. For the perovskite oxide, the electronic conduction is created by polaron hopping between the B-site cations and the oxygen ions via a mechanism similar to the Zerner double exchange process [19]. A conductivity of 23–40 S cm^{-1} was measured for BSCN in air between 300 and 900 °C, which is smaller than the conductivity of SCN, which is 120–80 S cm^{-1} [26]. For $Ba_{1-x}Sr_xCo_{0.8}Fe_{0.2}O_{3-\delta}$ composite oxides, we have demonstrated that the increase in Ba^{2+} content in the composite leads to a decrease in the electrical conductivity. This is due to an increase in the concentration of oxygen vacancies within the oxide lattice, which causes a barrier for electron hopping between the B-site cations and oxygen ions [9]. A similar explanation can be applied to BSCN.

An increase in electrical conductivity with temperature was observed for BSCN in air and other atmospheres with different oxygen partial pressures, demonstrating semiconductor-like behavior. Previously, we observed that SCN displayed metallic conduction behavior in air, which is characterized by a decrease in conductivity with temperature [24]. This suggests that the partial substitution of Sr^{2+} in SCN by Ba^{2+} altered the mechanism of electrical conduction in the composite oxide. A decrease in electrical conductivity was observed with reduced oxygen partial pressure for BSCN, suggesting P-type electronic conducting behavior. At an oxygen partial pressure of 10^{-2} atm, which is equal to an over potential of 0.057 V for the cathode in air, an electrical conductivity of 13–34 S cm^{-1} was maintained. This is only slightly lower than in an air atmosphere.

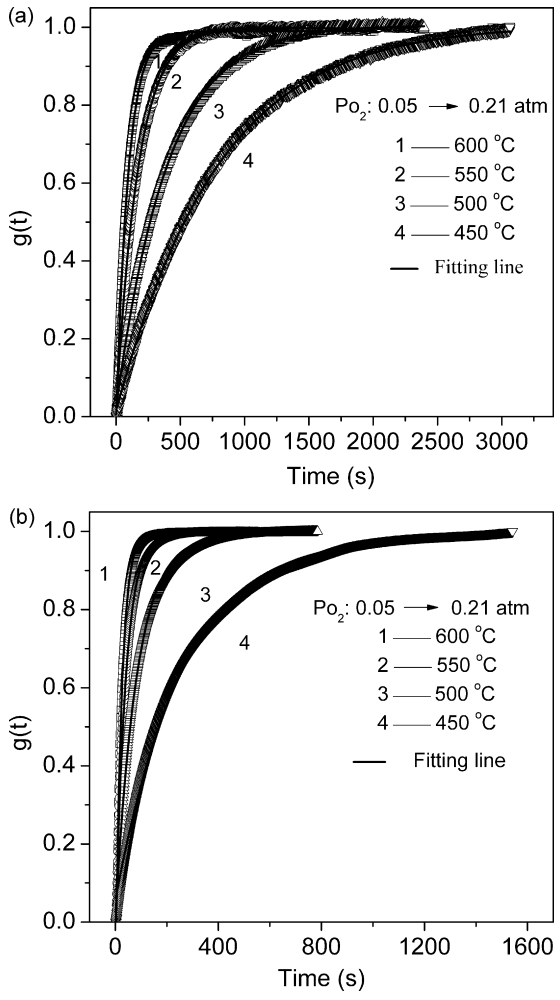

Fig. 7. ECR curves for SCN (a) and BSCN (b) at various temperatures after the oxygen partial pressure suddenly changed from 0.05 to 0.21 atm.

3.4. D_{chem} and k_{ex}

The electrode performance is closely related to the intrinsic properties of the electrode material, such as surface exchange kinetics and bulk diffusion properties. The chemical diffusion coefficient (D_{chem}) and surface exchange coefficient (k_{ex}) of BSCN and SCN were comparatively studied by an electrical conductivity relaxation technique. Fig. 7 shows the electrical conductivity relaxation curves of SCN and BSCN oxides at 600 °C by a sudden change in the oxygen partial pressure from 0.05 to 0.21 atm. D_{chem} and k_{ex} can be obtained by fitting the electrical conductivity relaxation curves into Eq. (1): [34]

$$g(t) = \frac{\sigma(t)-\sigma(0)}{\sigma(\infty)-\sigma(0)} = 1 - \sum_{n=1}^{\infty}\sum_{m=1}^{\infty}\sum_{p=1}^{\infty} \times \frac{2C_1^2 \exp(-\alpha_{1n}^2 D_{chem} t/l_1^2)}{\alpha_{1n}^2(\alpha_{1n}^2 + C_1^2 + C_1)} \times \frac{2C_2^2 \exp(-\alpha_{2m}^2 D_{chem} t/l_2^2)}{\alpha_{2m}^2(\alpha_{2m}^2 + C_2^2 + C_2)} \times \frac{2C_3^2 \exp(-\alpha_{3p}^2 D_{chem} t/l_3^2)}{\alpha_{3p}^2(\alpha_{3p}^2 + C_3^2 + C_3)} \quad (1)$$

where $\sigma(0)$, $\sigma(t)$ and $\sigma(\infty)$ denote the initial, time dependent and final conductivities, respectively. The parameters C_1, C_2 and C_3 are

Table 2
D_{chem} and k_{chem} for SCN and BSCN oxides at various temperatures obtained from ECR during the oxidation process.

Sample	T (°C)	D_{chem} ($cm^2\ s^{-1}$)	k_{chem} ($cm\ s^{-1}$)
SCN	600	2.7×10^{-5}	$8.5E \times 10^{-4}$
	550	1.6×10^{-5}	4.8×10^{-4}
	500	7.0×10^{-6}	2.1×10^{-4}
	450	3.5×10^{-6}	1.1×10^{-4}
BSCN	600	1.3×10^{-4}	3.3×10^{-5}
	550	7.9×10^{-5}	1.9×10^{-3}
	500	3.7×10^{-5}	8.3×10^{-4}
	450	1.2×10^{-5}	2.5×10^{-4}

defined as:

$$C_1 = \frac{l_1}{L_d} C_2 = \frac{l_2}{L_d} C_3 = \frac{l_3}{L_d} L_d = \frac{D_{chem}}{k_{ex}} \quad (2)$$

The coefficients a_{1n}, a_{2m} and a_{3p} are the roots of the transcendental equations:

$$C_1 = \pm_{1n} \tan \pm_{1n} C_2 = \alpha_{2m} \tan \alpha_{2m} C_3 = \alpha_{3p} \tan \alpha_{3p} \quad (3)$$

Table 2 summarizes the fitted D_{chem} and k_{ex} for both SCN and BSCN in the oxidation process (the sudden change of the oxygen partial pressure from 0.05 to 0.21 atm). At each temperature, k_{ex} is approximately one order of magnitude larger than the D_{chem} for BSCN and SCN. This suggests excellent surface exchange properties. Both the D_{chem} and k_{ex} for BSCN are larger than SCN, which suggests that BSCN may have higher electrochemical activity for oxygen reduction than SCN.

3.5. Symmetric cell performance

To demonstrate the electrochemical activity of BSCN for oxygen reduction, electrochemical impedance spectroscopy of a symmetric cell with BSCN electrodes was measured in air under OCV conditions. Fig. 8a presents a typical impedance spectrum at 600 °C in the Nyquist plot. The spectrum contains a tail at high-frequency, which is attributed to the inductance of the cell and at least two depressed semicircle. The high-frequency intercept of the impedance spectrum with the real axis gives the ohmic resistance of electrodes and the electrolyte, while the low-frequency intercept gives the total resistance of the cell ($R_{ohm} + R_P$). The difference between the intercept of the impedance spectrum with the real axis at high-frequency and the intercept at low-frequency represents the polarization resistance (R_P) of the two symmetric electrodes. Here the reported values have been obtained dividing by two the experimentally measured values in order to obtain the resistances of the single electrodes layer. Fig. 8b shows the temperature dependence of R_P for various BSCN electrodes fired at different temperatures in an Arrhenius plot. The firing temperature was found to have little influence on the ohmic resistance of the cell for a calcination temperature between 950 and 1050 °C. This implies the phase reaction between BSCN and SDC is not significant, which is in agreement with the powder reaction results, as shown in Fig. 2. Because there is no obvious phase reaction between BSCN and SDC, the increase in R_P at a calcination temperature of 1100 °C may be due to electrode sintering. After the firing at 1000 °C, a polarization resistance of around 0.1 $\Omega\ cm^{-2}$ was achieved for BSCN at 600 °C, which is comparable to the BSCF (0.055–0.071 $\Omega\ cm^{-2}$) [18] and SCN (0.094 $\Omega\ cm^{-2}$) [25] values reported in the literature and measured under similar conditions.

The cathodic polarization resistance may be due to charge transfer across the electrode–electrolyte interface and/or the air–electrode interface. The resistance may also be due to surface processes including oxygen surface adsorption, dissociation and surface diffusion. Based on results in the literature,

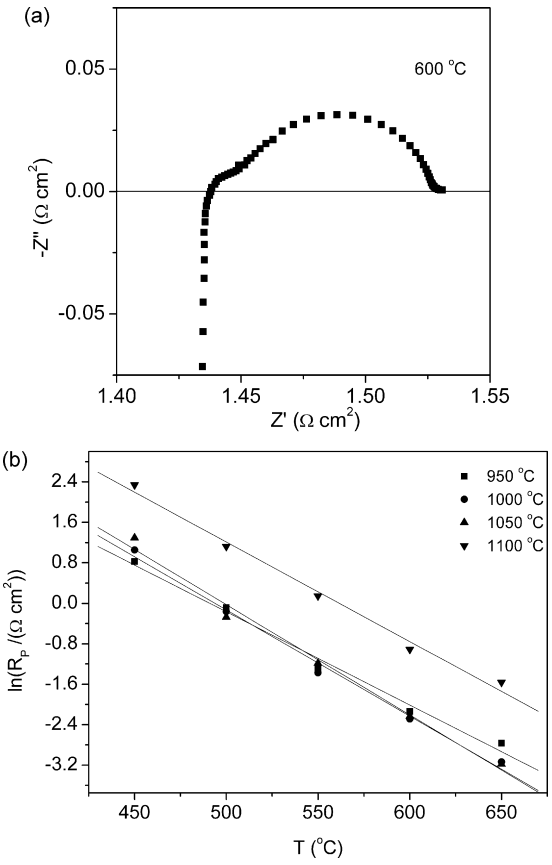

Fig. 8. Impedance spectroscopy of the BSCN cathode in the Nyquist plot measured at 600 °C (a) and R_P as a function of temperature for the BSCN cathode calcined at various temperatures for 2 h under air atmosphere (b).

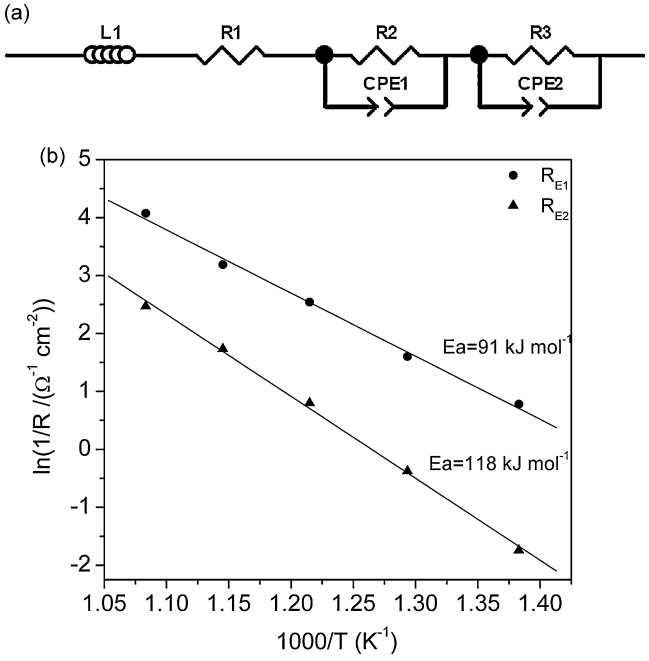

Fig. 9. Equivalent circuit used for fitting the impedance data measured under open circuit voltage condition (a) and the temperature dependence of $1/R_{E1}$ and $1/R_{E2}$ for the BSCN cathode (b).

Table 3
Characteristic frequencies associated with arc 1 and arc 2 of the EIS of the symmetric cell with the BSCN electrode at various oxygen partial pressures at 600 °C.

P_{O_2} (atm)	0.04	0.1	0.2	0.4	0.6	1
F_1 (Hz)	17862.24	18816.01	18609.49	17249.53	187228	22295.33
F_2 (Hz)	9.513435	13.80634	26.97825	31.71733	35.87861	42.0979

the high-frequency arc is likely associated with an ion charge transfer process at the electrolyte–electrode interface. The high-to-intermediate frequency arc is associated with the charge transfer process at the air–electrode interface and the intermediate-to-low-frequency arc is caused by oxygen surface adsorption, dissociation and surface diffusion [35–38]. It was found that the EIS of BSCN contains two separable depressed arcs, which can be fitted into an equivalent circuit as shown in Fig. 9a. The corresponding polarization resistances associated with these two arcs are designated R_{E1} and R_{E2}, respectively. The temperature dependence of R_{E1} and R_{E2} at various temperatures are shown in Fig. 9b. From the figure, it is observed that R_{E2} overwhelms R_{E1}, which indicates that the rate-limiting step is related to the process that occurs at the intermediate-to-low-frequency range. To obtain more insight into the oxygen reduction reaction over the electrode, the characteristic frequency f (which is a very useful tool for identifying oxygen reduction reaction processes), was calculated based on the equation $f = (RT^{1/p})^{-1/p}/2\pi$ [35,37]. Table 3 summarizes the fitted and calculated parameters as a function of the oxygen partial pressure under zero DC bias conditions at 600 °C. It was observed that the values of f for the high-frequency arc are similar to the reported values for oxide-ion transfer through the electrolyte–electrode interface [35,37]. The angular relaxation frequency of the intermediate frequency arc is between 9 and 42 Hz, which is in the typical range for a charge transfer process that occurs over the air–electrode interface [36]. Therefore, the first arc at the high-frequency range is likely associated with oxygen ion charge transfer across the electrolyte–electrode interface, while the second arc is likely related to charge transfer at the air–electrode interface.

To further clarify the oxygen reduction processes over the BSCN electrode, the electrode polarization resistance of BSCN was investigated under various oxygen partial pressures. In Fig. 10, the typical EIS in Nyquist plots (a) and the LnP_{O_2} dependence of Ln($1/R_P$) is shown in Fig. 10(b–d). For different processes, there is a unique

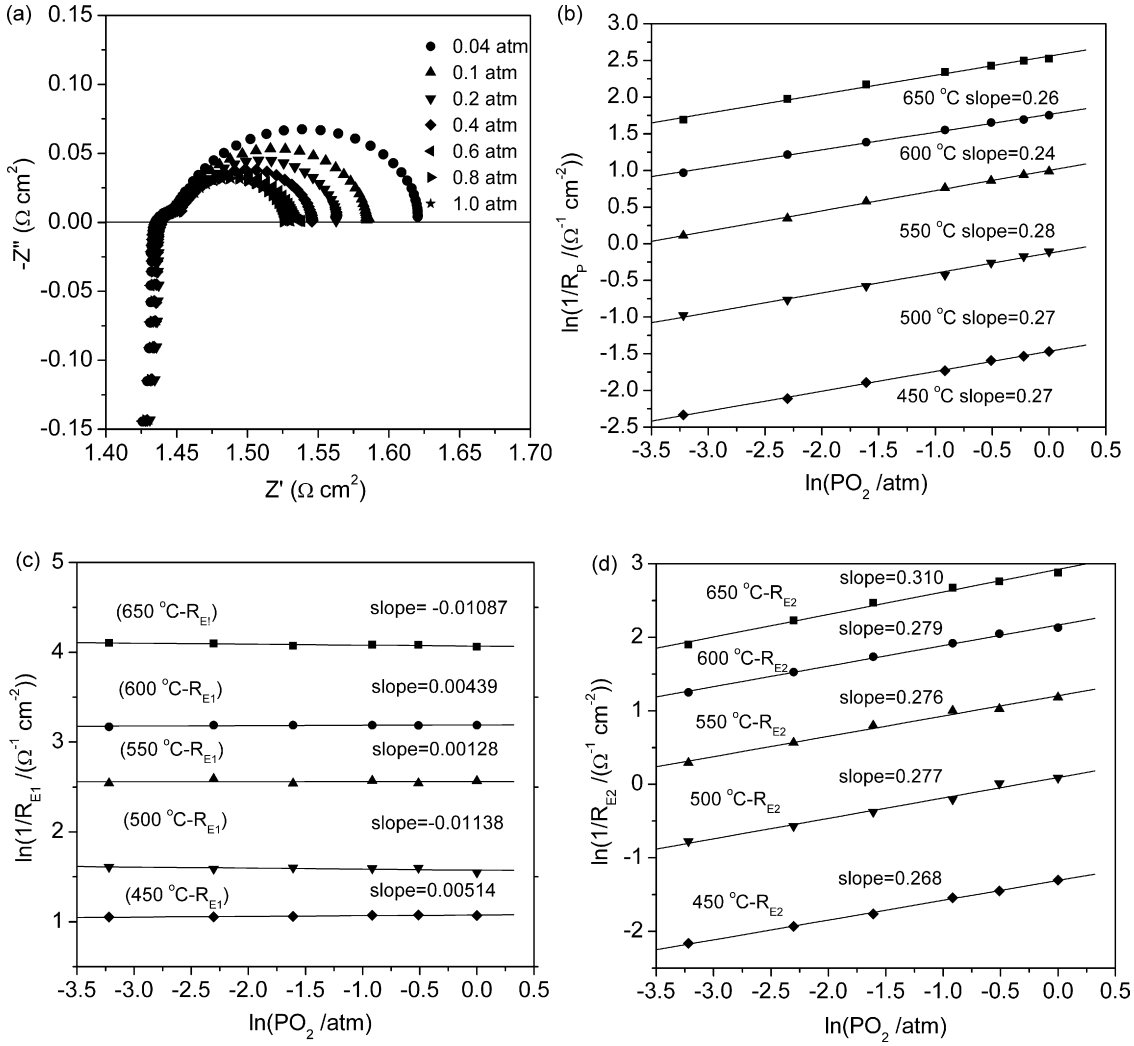

Fig. 10. Impedance spectroscopy in the Nyquist plot for the BSCN cathode at various oxygen partial pressures measured at 600 °C (a), and $1/R_P$ (b), $1/R_{E1}$ (c) and $1/R_{E2}$ (d) of the BSCN cathode as a function of the oxygen partial pressure tested from 650 to 450 °C.

dependence of $\mathrm{Ln}(1/R_P)$ with respect to $\mathrm{Ln}P_{O_2}$. A value of 0.5, 0.25 or 0 is associated with the following reactions respectively [36].

$$O_{2,ads} \Leftrightarrow 2O_{0,ads}$$

(Oxygen surface adsorption, dissociation and surface diffusion)

$$O_{ads} + V^{\bullet\bullet}_{0,electrode} + 2e' \Leftrightarrow O^{\times}_{0,electrode}$$

(Surface diffusion and charge transfer)

$$O^{\times}_{0,electrode} + V^{\bullet\bullet}_{0,electrolyte} \Leftrightarrow O^{\times}_{0,electrode} + V^{\bullet\bullet}_{0,electrode}$$

(Ion charge transfer)

Between 450 and 650 °C, a value of 0 for R_{E1} indicates a process involving ion charge transfer from electrode to electrolyte [36]. A slope of approximately 0.31 for R_{E2} was obtained for the BSCN electrode. This implies that the contribution of polarization resistances, R_{E2}, is mainly due to the charge transfer process. It further suggests that oxygen reduction over the BSCN electrode is rate-limited by the relatively slow charge transfer process due to its low electrical conductivity.

3.6. Single cell performance

To test the cathodic performance of BSCN under real fuel cell conditions, an anode-supported thin-film electrolyte fuel cell with an Ni + SDC anode (~600 μm), SDC electrolyte (~20 μm) and BSCN cathode (~40 μm) was fabricated. Shown in Fig. 11a are the typical *I–V* polarization curves of the fuel cells at various temperatures.

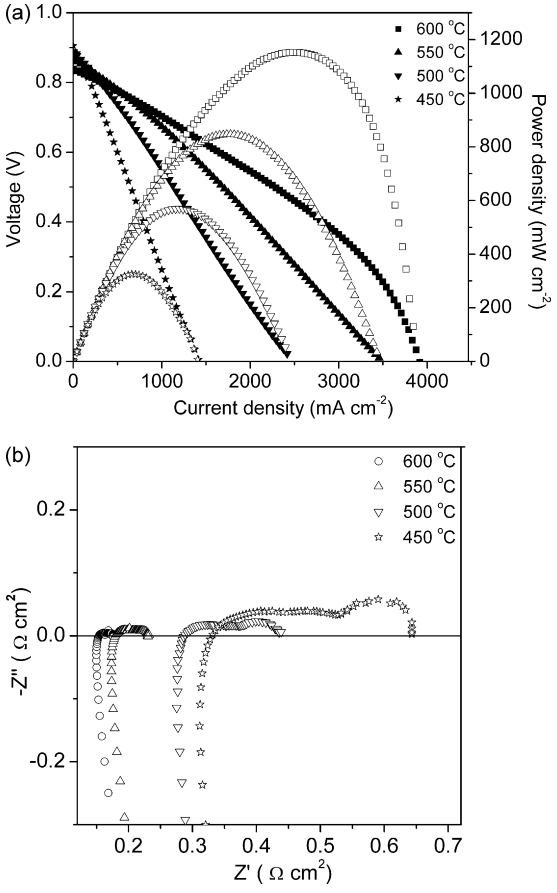

Fig. 11. *I–V* and *I–P* curves for a SOFC with a BSCN cathode fired at 1000 °C (a), and the corresponding impedance spectra of the cell measured under OCV conditions.

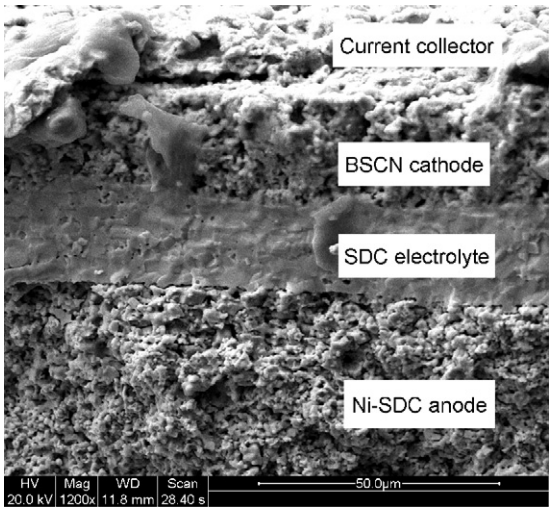

Fig. 12. SEM image from a cross-sectional view of the cell after *I–V* and *I–P* tests.

The corresponding EIS of the cell under OCV conditions are shown in Fig. 11b. A peak power density of ~1150 mW cm^{-2} was achieved at 600 °C, which is higher than reported similar cells with common cathode materials for oxygen-ionic SOFCs, for example, a peak power density of 422 mW cm^{-2} was achieved at 600 °C by Leng et al. with a composite cathode of LSCF and GDC [39]. However, at high polarization current density (>3 A cm^{-2}), a significant concentration polarization occurred due to insufficient cathode porosity. At temperatures below 550 °C, a linear response of the cell voltage to the polarization current density suggests that the concentration polarization disappeared. At 450 °C, a peak power density of 300 mW cm^{-2} was achieved. Compared to the results for similar fuel cells with SCN as the cathode [25], the fuel cell with the BSCN cathode delivered a slightly higher performance. As shown in Fig. 11b, under OCV conditions, the cell resistance at 600 and 550 °C is mainly due to the ohmic resistance. This implies that a reduction in the thickness of the electrolyte may further increase the cell power output. At 450 °C, the electrode polarization resistance (0.33 Ω cm^{-2}) is comparable to the electrolyte ohmic resistance (~0.32 Ω cm^{-2}).

Fig. 12 shows the SEM photo of the cell after the *I–V* polarization test from a cross-sectional view. The cathode layer is denser than the anode layer, which explains the appearance of concentration polarization at high current density at 600 °C. After the fuel cell test, the cathode still adhered to the electrolyte surface without evidence of delamination. This suggests that the BSCN cathode matched the SDC electrolyte. This is likely due to the small difference in TEC for BSCN and SCN (Fig. 4) between 200 and 600 °C.

4. Conclusions

BSCN was successfully used as a cathode for a SOFC operated at temperatures between 450 and 600 °C. The phase reaction between BSCN and SDC is not significant at temperatures up to 1100 °C based on the powder reaction test. There is also no evidence of an interfacial layer between the BSCN cathode and the SDC electrolyte according to SEM results. The relatively small TEC (14.4×10^{-6} K^{-1}, 200–500 °C) of BSCN ensured the attachment of the BSCN cathode layer to the SDC electrolyte surface, even after fuel cell operations. Through the electricity conductivity relaxation test, BSCN proved to have a higher D_{chem} and k_{ex} than SCN. Although oxygen reduction over the BSCN electrode is rate-limited by the relatively slow charge transfer process due to its low electrical conductivity (which is 23–40 S cm^{-1} in air between 300 and 900 °C), a small electrode polarization resistance of around 0.1 Ω cm^{-2} was achieved for the

BSCN cathode at 600 °C, which is comparable to BSCF and SCN cathodes. At 600 °C, a thin-film electrolyte SOFC with a BSCN cathode delivered a peak power density of ~1150 mW cm^{-2}. At 450 °C, a peak power density of 300 mW cm^{-2} was also achieved. These results suggest that BSCN is a highly promising cathode for IT-SOFCs with a SDC electrolyte.

Acknowledgements

The work is supported by the National Natural Science Foundation of China under contract Nos. 20676061 and 20703024, by the National 863 Program under contract No. 2007AA05Z133 and by the National Basic Research Program of China under Contract No. 2007CB209704.

References

[1] H.Q. Jiang, H.H. Wang, S. Werth, T. Schiestel, J. Caro, Angew. Chem. Int. Ed. 120 (2008) 9481–9484.
[2] Y.P. Lu, A.G. Dixon, W.R. Moster, Y.H. Ma, U. Balachandran, J. Membr. Sci. 170 (2000) 27–34.
[3] S. Pei, M.S. Kleefisch, T.P. Kobylinski, J. Faber, C.A. Udovich, Catal. Lett. 30 (1995) 201–212.
[4] H.J.M. Bouwmeester, Catal. Today 82 (2003) 141–150.
[5] Y. Teraoka, H.M. Zhang, K. Okamoto, N. Yamazoe, Mater. Res. Bull. 23 (1988) 51–58.
[6] V.V. Kharton, E.N. Naumovich, A.V. Nikolaev, J. Membr. Sci. 111 (1996) 149–157.
[7] S. Lee, K.S. Lee, S.K. Woo, Solid State Ionics 158 (2003) 287–296.
[8] Y. Teraoka, H. Shimokawa, Ch.Y. Kang, Solid State Ionics 177 (2006) 2245–2248.
[9] P.Y. Zeng, Z.H. Chen, W. Zhou, H.X. Gu, Z.P. Shao, S.M. Liu, J. Membr. Sci. 291 (2007) 148–156.
[10] J. Sunarso, S. Baumann, J.M. Serra, J. Membr. Sci. 320 (2008) 13–41.
[11] J.M. Serra, V.B. Vert, O. Buchler, Chem. Mater. 20 (2008) 3867–3875.
[12] H.C. Yu, K.Z. Fung, Mater. Res. Bull. 38 (2003) 231–239.
[13] J.W. Stevenson, T.R. Armstrong, R.D. Carneim, W.J. Weber, J. Electrochem. Soc. 143 (1996) 2722–2729.
[14] C.R. Xia, W. Rauch, F.L. Chen, M.L. Liu, Solid State Ionics 149 (2002) 11–19.
[15] S.J. Skinner, Int. J. Inorg. Mater. 3 (2001) 113–121.
[16] R. Chiba, F. Yoshimura, Y. Sakural, Solid State Ionics 124 (1999) 281–288.
[17] Z.P. Shao, W.S. Yang, Y. Cong, H. Dong, J.H. Tong, G.X. Xiong, J. Membr. Sci. 172 (2000) 177–188.
[18] Z.P. Shao, S.M. Haile, Nature 134 (2004) 170–173.
[19] P.Y. Zeng, R. Ran, Z.H. Chen, W. Zhou, H.X. Gu, Z.P. Shao, S.M. Liu, J. Alloys Compd. 455 (2008) 465–470.
[20] W. Zhou, Z.P. Shao, R. Ran, R. Cai, Electrochem. Commun. 10 (2008) 1647–1651.
[21] W. Zhou, B.M. An, R. Ran, Z.P. Shao, J. Electrochem. Soc. 156 (2009) B884–B890.
[22] T. Nagai, W. Ito, T. Sakon, Solid State Ionics 177 (2007) 3433–3444.
[23] W. Ito, T. Nagai, T. Sakon, Solid State Ionics 178 (2007) 809–816.
[24] K. Zhang, R. Ran, L. Ge, Z.P. Shao, W.Q. Jin, N.P. Xu, J. Membr. Sci. 323 (2008) 436–443.
[25] W. Zhou, Z.P. Shao, R. Ran, W.Q. Jin, N.P. Xu, Chem. Commun (2008) 5791–5793.
[26] J. Zhao, K. Zhang, D. Gao, Z.P. Shao, S.M. Liu, Sep. Purif. Technol. 71 (2010) 152–159.
[27] A. Mitterdorfer, L.J. Gauckler, Solid state Ionics 111 (1998) 185–218.
[28] S. Sameshima, T. Ichikawa, M. Kawaminami, Y. Hirata, Mater. Chem. Phys. 61 (1999) 31–35.
[29] S. Uhlenbruck, F. Tietz, Mater. Sci. Eng. B107 (2004) 277–282.
[30] M. Radovic, S.A. Speakman, L.F. Allard, E.A. Payzant, E. Lara-Curzio, W.M. Kriven, J. Lloyd, L. Fegely, N. Orlovskaya, J. Power Sources 184 (2008) 77–83.
[31] B. Wei, Z. Lu, X.Q. Huang, J.P. Miao, X.Q. Sha, X.S. Xin, W.H. Su, J. Eur. Ceram. Soc. 26 (2006) 2827–2832.
[32] A. Petric, P. Huang, F. Tietz, Solid State Ionics 135 (2000) 179–725.
[33] W. Zhou, R. Ran, Z.P. Shao, Acta Mater. 56 (2008) 2687–2698.
[34] I. Yasuda, M. Hishinuma, J. Solid State Chem. 123 (1998) 382–390.
[35] D.J. Chen, R. Ran, K. Zhang, J. Wang, Z.P. Shao, J. Power Sources 188 (2009) 96–105.
[36] Y. Takeda, R. Kanno, M. Noda, Y. Tomida, O. Yamamoto, J. Electrochem. Soc. 134 (1987) 2656–2661.
[37] M.J. Escudero, A. Aguadero, J.A. Alonso, L. DAza, J. Electroanal. Chem. 611 (2007) 107–116.
[38] S.W. Baek, J. Bae, Y.S. Yoo, J. Power Sources 193 (2009) 431–440.
[39] Y.J. Leng, S.H. Chan, Q.L. Liu, Int. J. Hydrogen Energy 33 (2008) 3808–3817.